Filtration of Particulate Suspensions in Acoustically Driven Porous Media

Sanjay Gupta and Donald L. Feke
Dept. of Chemical Engineering, Case Western Reserve University, Cleveland, OH 44106

Retention of suspended solids within a porous medium subjected to resonant ultrasonic fields was studied experimentally. In laboratory tests, 325 mesh polystyrene particles were collected with high (typically > 80%) single-pass efficiency using a polyester foam mesh with pores more than two orders of magnitude larger than the particles retained. Deactivation of the acoustic field allows the retained particles to be flushed from the porous medium. The effects on filtration efficiency of processing variables (suspension flow rate, solids concentration in the feed, intensity of the acoustic field, and frequency of the acoustic field) are reported. A simplified analysis of particle trajectories toward cylindrical collectors in response to acoustic and hydrodynamic forces provides insight into the fundamental physical phenomena that govern the acoustically enhanced filtration process.

Introduction

Many chemical, material, and biological processes involve multiphase systems where a fluid phase is the carrier for a particulate or immiscible liquid phase. Very often, finely divided dispersions are deliberately created to aid heat- and mass-transfer rates by utilizing the large surface area to volume ratio of the dispersed phase. Normally, at one or more stages in these processes, there is a need for separation of the dispersed from the continuous phase, and various methods have been developed to meet this need. Conventional approaches include physical screening techniques (mechanical sieves, beds of filtration media, or filter membranes) and gravity-driven methods (settling or flotation) that accomplish the desired separation using the density difference between the dispersed and continuous phase. More advanced schemes utilize external fields (such as centrifugal, electrical, or magnetic) to enhance the quality or rate of separation.

In a recent article (Gupta and Feke, 1997), we described and demonstrated a novel separation process that falls into this latter category. Specifically, we apply an ultrasonic standing-wave field within a highly porous medium. The acoustic field allows the collection of suspended solids two or three orders of magnitude smaller than the pore size of the porous medium. Thus, collection of micron-sized solids can be achieved without the large pressure drop penalty usually associated with filtration of such solids. Also, cleaning and regeneration of the filtration medium is readily achieved by deactivating the acoustic field and flushing the collected solids from the porous medium with processing fluid. In this article, we provide further experimental data demonstrating this process and a simplified analysis of the trajectory of particles toward cylindrical fibers, which provides some theoretical basis for the method.

In the past few decades, various methods based on the use of ultrasonic standing-wave fields have been developed for separation of fine particles from liquid streams (see, e.g., Tolt and Feke, 1993; Mandralis et al., 1994; Mandralis and Feke, 1993a; Apfel, 1990; Schram and Rendell, 1989; Peterson, 1988; Schram, 1988; Yasuda et al., 1995). These methods utilize the density and/or compressibility difference between the dispersed phase and the host liquid to yield sharp and efficient separations. In most of these methods, a one-dimensional sound field is used to organize particles of a suspension into thin parallel bands separated by a one-half acoustic wavelength spacing. The particles are recovered by either using closely spaced physical barriers between the bands of particles (Mandralis et al., 1994; Mandralis and Feke, 1993a, 1993b; Gupta et al., 1995), transporting particles in the opposite direction of the flowing host liquid by using pseudo-standing waves (Tolt and Feke, 1992; Benes et al., 1991), or relying on gravity to settle the swarms of particles organized by the acoustic field (Whitworth et al., 1991; Frank et al.,

Present address of S. Gupta: Nestle R&D Center, Marysville, OH 43040.
Correspondence concerning this article should be addressed to D. L. Feke.

1993; Allman and Coakley, 1994; Doblhoff-Dier et al., 1994). Many of the hurdles associated with practical applications of these techniques, such as strict mechanical clearances between physical barriers or slow sedimentation rates, are absent in our new technique.

The separation method reported here is a blend of acoustic and physical screening methods. In our earlier article (Gupta and Feke, 1997) we reported the results of experiments in which two types of porous media were used: an unconsolidated bed of millimeter-scale glass beads and aluminum meshes of various pore sizes. The various acoustic phenomena that may be responsible for particle entrapment were also discussed. In this article, we examined the use of highly porous polymeric foam as the filtration medium. In contrast to glass and aluminum, this material has an acoustic impedance close to that of the water, which was used as the suspension medium in the demonstration experiments. Therefore acoustic scattering within the porous medium is expected to be reduced compared to the previous studies.

Experimental Studies

Equipment

The filtration experiments were carried out in a rectangular acoustic chamber, which is shown in Figure 1. The acoustic chamber consisted of a rectangular lead zirconate titanate (PZT) transducer (APC 880, $76.2 \times 38.1 \times 6.25$ mm, fundamental frequency 320 kHz, from American Piezo Ceramics, Inc., Mackeville, PA) mounted in an aluminum frame. A glass plate of similar lateral dimensions, mounted in a similar plexiglas frame, served as reflector. The two frames were placed parallel to each other at either 5.8- or 12.2-mm spacing in a Plexiglas channel (also constructed from plates). Polyester foam having ten pores per inch (ppi) (0.4 pore/mm) and porosity greater than 0.9 (Stephenson & Lawyer, Inc., Grand Rapids, MI) was used as the filtration medium. For all experiments reported here, the dimensions of the porous region were 70 mm high, 35 mm wide, and 5.82 or 12.2 mm thick in the direction of propagation of acoustic field. The chamber was equipped with ports for suspension feed (bottom of the chamber) and filtrate removal (top of the chamber). In all cases, the porous medium was supported on a 17.5-mm-high metallic mesh positioned below the acoustically active region, to help the feed distribution within the chamber.

The ultrasonic field was produced by energizing the transducer at 1.103 MHz (or a higher harmonic) frequency using a continuous signal generated by a KROHN-HITE 2100 A signal generator and amplified by a ENI 240 L power amplifier. The operating frequency corresponds to one of the resonance frequencies of the acoustic chamber when it is filled with fluid, but with no porous medium installed. The electrical power consumption was measured by a Bird Wattmeter Model 4410 A.

Aqueous suspensions of 325-mesh (particle radius in the range of 2 to 30 μm) polystyrene divinyl benzene particles were used as the test suspensions for filtration experiments. Since the particles are small and their mass density (1.05 g/cm^3) is close to water, the effect of gravity on the stability of the suspension may be ignored. These particles are known to have a low acoustic contrast (in water), $F = 0.23$ (Gupta et al., 1995), so these suspensions are a severe test for the acoustic separation method. The particles were suspended in deionized water using Triton X-100 surfactant. A peristaltic pump and a flow integrator combination was used to deliver the suspension to the acoustic chamber. The flow integrator works as a sump and reduces the flow pulsation. Particle concentration in suspensions was determined by measuring the light absorbance in a Spectronic 1001 Plus (Milton Roy) photometer. The absorbance values were converted to weight-percentage solids using calibration curves determined from measurements on standard suspensions.

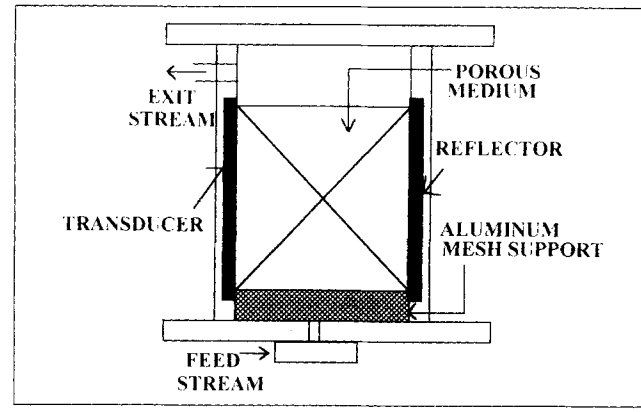

Figure 1. Acoustic chamber used in the experiments.

Procedure

Feed suspensions of known concentration of polystyrene particles in water (ranging from 0.5 wt. % to 1.0 wt. %) were passed through the acoustic chamber at fixed flow rates (ranging from 30 cm^3/min to 60 cm^3/min). The chamber was energized with 20 to 50 W of power delivered to the transducer.

Typically, experiments were conducted by first establishing a flow of suspension through the chamber before the acoustic field was propagated. Following activation of the field, the particle concentration in the exit stream at the top of the chamber was measured at regular intervals of one-half to one minute. Small samples of effluent (approximately 5 cm^3) were collected and immediately analyzed using the spectrometer. The clock for each experiment was started from the instance of activating the acoustic field.

Experimental Results and Discussion

Visual results

Visual observations of the filtration phenomena were recorded on a videocassette with a Tamron 90 mm, F/2.5 lens attached on an Olympus CCD camera. Figure 2 shows the view into the acoustic chamber through the glass reflector while suspsension is fed through the porous barrier from bottom to top. Table 1 lists the process parameters for these demonstration experiments.

When no acoustic field is applied (Figure 2a), the small polystyrene particles cannot be easily observed within the porous barrier, and suspension flows through the chamber essentially unimpeded by the barrier. However, when the acoustic field is energized, the retention of the particles within

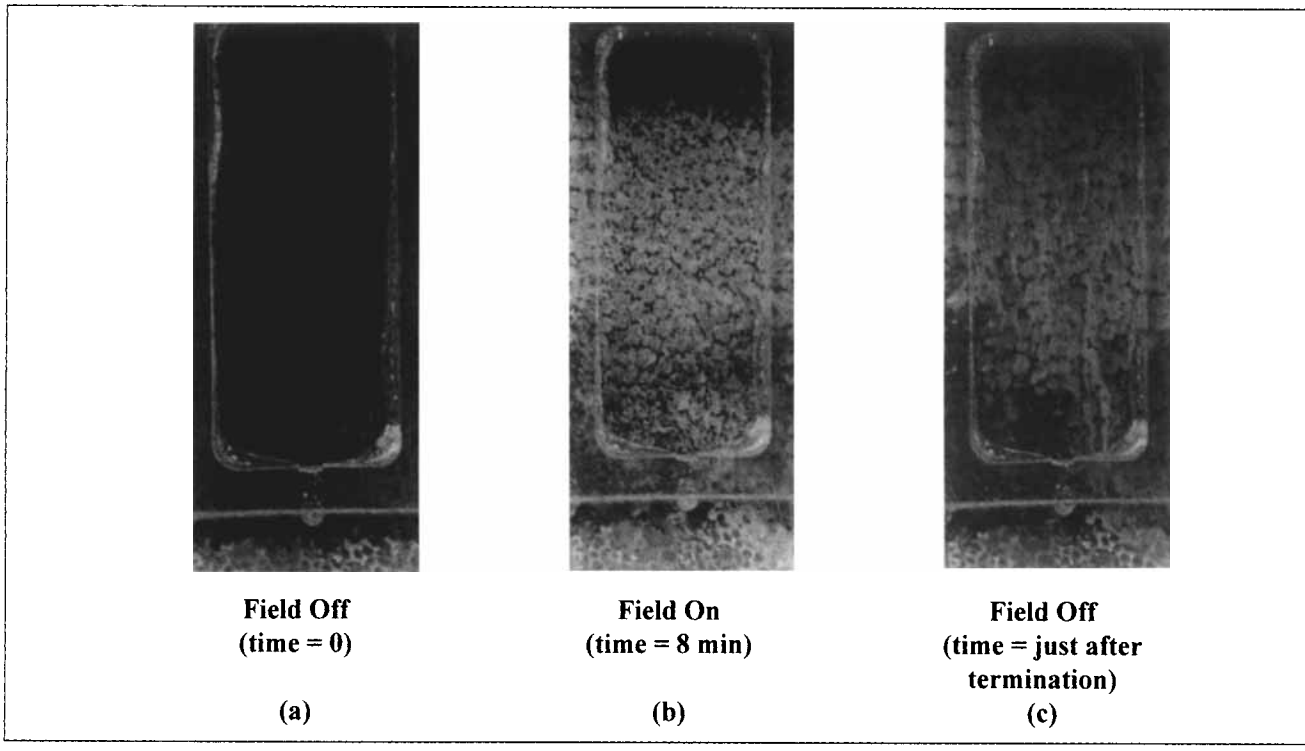

Figure 2. Visual results for the 10-ppi polymer foam as the porous medium.

(a) Acoustic field off; (b) acoustic field on; (c) acoustic field terminated while fluid flow continues.

the porous barrier is quite obvious (Figure 2b). Collection of the particles into dendritic or globular configurations was observed. As suspension is continuously fed to the chamber, a distinct trapping zone is observed; the front of this zone moves from the bottom toward the top of the chamber, forming a saturated region within the porous barrier. If the acoustic field is deactivated (Figure 2c), the organized collection of the particles breaks down and the particles can immediately be flushed out with continued fluid flow.

Analogous photographs of the filtration performance using aluminum mesh or glass beads as the porous medium can be found in Gupta (1997).

Filtration performance

Unless stated otherwise, results are reported for the case when the transducer and reflector are kept 5.8 mm apart. Figure 3 shows typical results of the variation of the particle concentration in the exit stream with time. Here, a 0.5 wt. % suspension was fed at 40 cm^3/min to a chamber operated with 20 W of power.

Since the acoustic field is activated only after the suspension flow is established, the particle concentration in the effluent matches that of the feed concentration at the start of the experiment. The effluent concentration drops down to one-fifth of the feed concentration within one minute of operation, indicating that significant particle retention occurs within the porous medium. These results are equivalent to a cumulative retention efficiency of 80–90%. After a critical amount of solids has been collected within the porous medium (after 6–7 min of operation in this experiment), a saturation phenomenon is exhibited. Abrupt changes in concentration are observed in the effluent stream for short bursts, and in the intervening periods, additional particle collection occurs within the porous barrier. Visual observations indicate that the bursts of particles seen in the effluent stream are associated with large-scale coordinated vibrations and fluctuations of the collections of particles within the barrier.

Table 1. Experimental Conditions for Visual Demonstrations

Process parameter	Value
Transducer to reflector spacing	5.8 mm
Acoustic frequency	1.103 MHz
Suspension flow rate	35 cm^3/min
Feed concentration	0.5 wt. %
Electrical power	25 W

Figure 4 shows the effect of suspension feed rate on filtration efficiency for a 0.5 wt. % feed and a chamber operated at 20 W. Feed flow rates ranged from 30 cm^3/min to 60 cm^3/min, which corresponds to superficial velocities through the porous medium ranging from 0.25 cm/s to 0.50 cm/s. With an increase in feed rate, the residence time of the suspension in the acoustic field is reduced, and filtration efficiency correspondingly declines. In addition, time to saturation diminishes with increasing flow rate, indicating that filtration is limited by the space available for particle retention in the porous medium.

Figure 5 shows the influence of feed concentration on filtration efficiency for a set of experiments for which flow rate was fixed at 30 cm^3/min and electrical power supplied was 20 W. There is no significant difference in filtration efficiency until the porous medium becomes saturated. The saturation time appears to be roughly inversely proportional to the feed

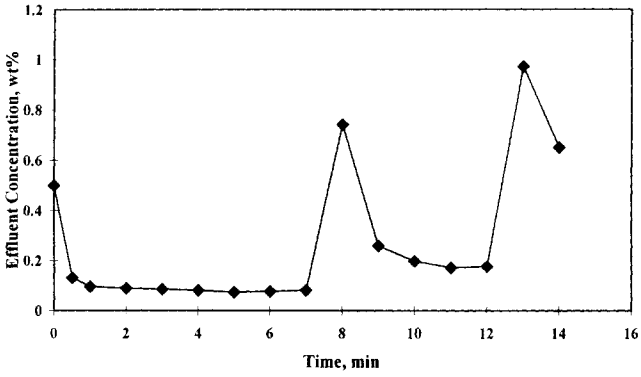

Figure 3. Typical experimental results for the effluent concentration as a function of time using the polymer foam.

A 0.5 wt. % suspension was fed at 40 cm^3/min, while the applied power was 20 W.

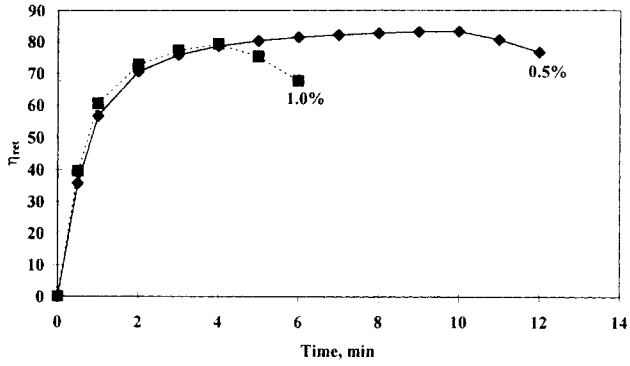

Figure 5. Effect of suspension concentration on the filtration performance.

Shown is the cumulative percentage of mass retained as a function of time. Experiments were conducted with two suspensions of 0.5 wt. and 1.0 wt. %, which were fed at 30 cm^3/min to a chamber energized with 20 W of power.

concentration, changing from 10 min for 0.5 wt. % feed to 4 min for 1.0 wt. % feed.

Figure 6 shows the effect of acoustic-field intensity, expressed as the electrical power delivered to the piezoelectric transducer, on filtration efficiency. The operating conditions for these experiments were set as a flow rate of 80 cm^3/min (superficial velocity of 0.65 cm/s) and a feed concentration of 0.5 wt. %. The performance improves as the power is increased from 20 W to 40 W, but there is no significant improvement in efficiency going to 50 W. At a high power such as 50 W, acoustic streaming might offset the effect of acoustic forces, and filtration efficiency can degrade. This indeed was observed in certain experiments.

One manner for scale-up of this new filtration process would be to increase the spacing between the transducer and reflector, and thus enable higher volumetric throughput at a fixed superficial velocity. Figure 7 shows the results of experiments conducted using two different gaps between the transducer and reflector on the collection efficiency. The operating conditions for these experiments were flow rates of 40 cm^3/min (for the 5.8-mm gap) and 80 cm^3/min (for the 12.8-mm gap), feed concentration of 0.5 wt. %, and power supplied of 20 and 40 W. At a fixed electrical power, an increase in the gap between the transducer and reflector causes a decrease in acoustic-field intensity that should lead to a degradation in filtration performance, as is seen in Figure 7. However, increasing the applied power can overcome this effect. As shown in the figure, doubling the power to 40 W for operation with the 12.5-mm gap leads to filtration efficiencies comparable to those obtained using 20 W of power with the smaller gap configuration.

Both primary and secondary acoustic forces increase with increasing frequency. Therefore, at a fixed power, one would expect an improvement in filter performance if the chamber were operated at a higher harmonic frequency, provided that the acoustic wavelength is still larger than the particle size, so that primary acoustic forces act. Figure 8, however, shows the opposite result for the experimental conditions of flow rate of 30 cm^3/min, feed concentration of 0.5 wt. %, and power of 20 W. The captured particles were observed to form a finer and crispier dendritic structure, which is consistent with the finer spatial variation in the acoustic field expected at the higher frequencies. At the higher harmonic, the porous medium became saturated at shorter times compared to that for the lower frequency, but the rate of particle capture in the initial period of filtration was not different for the two

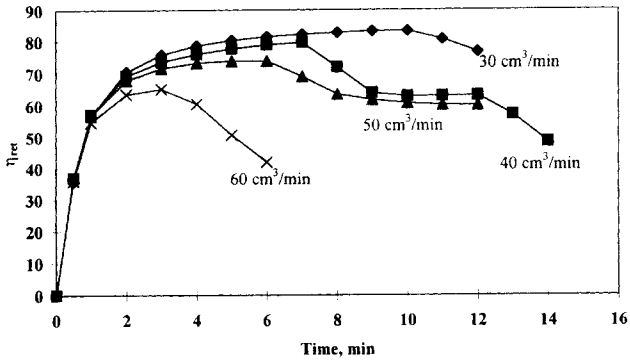

Figure 4. Effect of suspension feed rate on the filtration performance.

Cumulative filtration efficiency for a 0.5 wt. % feed suspension flowing through the chamber in the range 30 to 60 cm^3/min. The chamber was operated with 20 W of power.

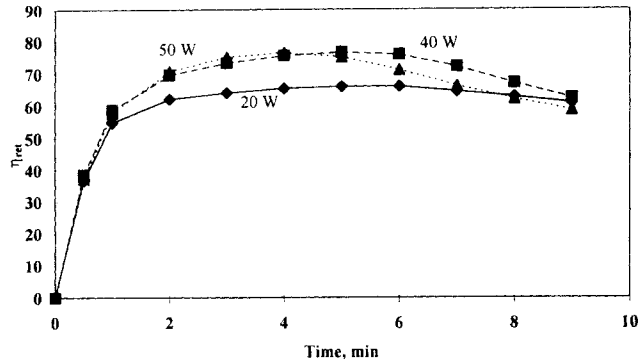

Figure 6. Effect of power on the filtration performance.

Shown is the cumulative percentage of particle mass retained by the filter as a function of time. A 0.5 wt. % suspension was fed at a rate of 80 cm^3/min. The applied power ranged from 20 to 50 W.

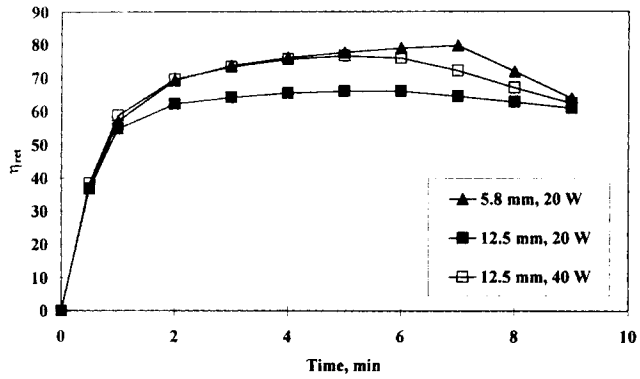

Figure 7. Effect of gap between transducer and reflector and power on the filtration performance.

Cumulative percentage of mass retained as a function of time. Experiments were conducted with gaps of 5.8 or 12.5 mm, flow rates 40 or 80 cm^3/min, and power levels of 20 or 40 W.

cases. Although the higher frequency was observed to have a detrimental effect on overall filtration efficiency for the polystyrene suspension used in these experiments, the results could be different, depending upon the particle-size distribution in the feed. A higher frequency may be more efficient in removal of smaller particles, for example.

Trajectory Analysis

In order to model the particle collection phenomenon, an expression for the acoustic radiation force on a particle inside the porous medium is needed. The propagation of acoustic waves in fluid-saturated porous media has been studied extensively since Biot developed the basic theory (Biot, 1956a,b). Biot and many other authors (e.g., Johnson, 1986) treat a saturated porous medium system as a continuous fluid interpenetrated by a continuous solid network. Using conservation equations, the acoustic-wave velocity and attenuation coefficients have been predicted as a function of physical properties of the system. However, the existing lumped-parameter models of porous media seldom include

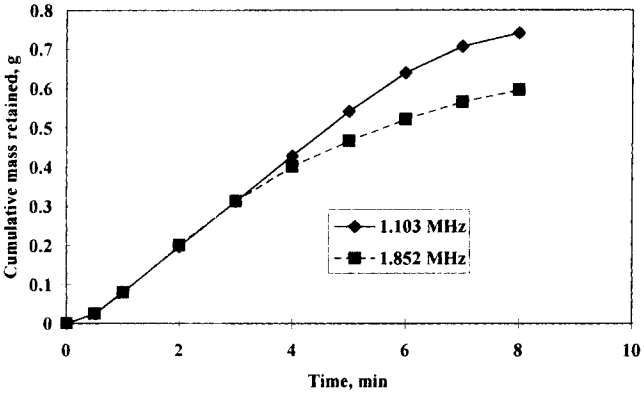

Figure 8. Effect of acoustic frequency on cumulative mass retained in the chamber.

A 0.5 wt. % suspension was fed at 30 cm^3/min. The chamber was operated at 1.103 or 1.852-MHz frequency with 20 W of power.

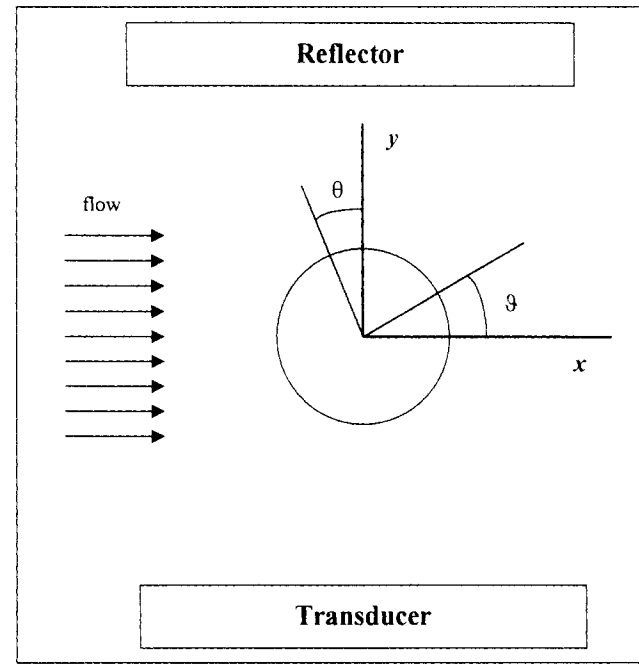

Figure 9. Geometry definition sketch used in the trajectory analysis.

microstructural details. Therefore, we first develop an appropriate expression for the acoustic radiation force. In conjunction with consideration of the hydrodynamic drag acting on particles, this will be used to formulate particle trajectory equations. As a first step toward a complete analysis of the filtration process, we consider here particle collection near a single fiber that represents one element of the porous medium.

Figure 9 provides a definition sketch for the trajectory analysis. An infinitely long cylindrical fiber of radius R_c is placed in a uniform steady flow field perpendicular to the axis of cylinder. Far away from the cylinder surface, the fluid has a uniform velocity U_f. A resonant planar one-dimensional acoustic field of wavenumber k and energy density E_{ac} is also assumed to be present in the same region. The direction of the acoustic-wave vector is orthogonal to both the flow direction and the axis of cylinder (the y-direction in Figure 9). Particles of radius R_p are carried along with the fluid toward the fiber.

Several assumptions are made in the derivation of the force-balance equations: (1) creeping flow around the cylinder; (2) the flow field is not affected by the presence of the particles; (3) the gravitational force is neglected because of the small particle size and small density difference (= 0.05 g/cm^3) between the particles and the fluid; (4) suspensions are dilute enough such that there is no hydrodynamic or acoustical interactions between particles; (5) particle inertia is negligible; and (6) steady state. The first assumption can be justified by considering a typical value of Reynolds number based on experimental conditions. For a 100-μm radius fiber, a flow speed of 0.002 m/s, and water as the suspending medium (density = 10^3 kg/m^3, viscosity = 10^{-3} Pa·s), the Reynolds number is 0.4.

Using these assumptions, a force balance on a given particle reduces to

$$\boldsymbol{F}_{ac} + \boldsymbol{F}_D = \boldsymbol{0}, \tag{1}$$

where $\boldsymbol{F}_{ac}$ is the primary acoustic force and $\boldsymbol{F}_D$ is the hydrodynamic drag force. The latter is given by Stokes' law as

$$\boldsymbol{F}_D = 6\pi\mu R_p(\boldsymbol{u}_f - \boldsymbol{u}_p), \tag{2}$$

where μ is the fluid viscosity, $\boldsymbol{u}_f$ is the fluid velocity, and $\boldsymbol{u}_p$ is the particle velocity.

Acoustic Force

King (1934) first calculated the acoustic force on a small rigid spherical particle in an inviscid fluid by solving the problem of flow around a small sphere in a sound field. Yosioka and Kawasima (1955) extended this analysis for the case of a compressible sphere. Gor'kov (1962) derived a very useful general expression for force on a particle in any kind of acoustic field (except a pure traveling wave) by integration of the momentum flux density tensor. This is given by the negative gradient of the acoustic potential, U

$$\boldsymbol{F}_{ac} = -\nabla U, \tag{3}$$

where

$$U = 2\pi R_p^3 \rho_f \left\{ \frac{\langle P_{in}^2 \rangle}{3\rho_f^2 c_f^2} f_1 - \frac{\langle \boldsymbol{V}_{in}^2 \rangle}{2} f_2 \right\}. \tag{4}$$

Here ρ_f is the fluid density, c_f the longitudinal sound speed in fluid, P_{in} and $\boldsymbol{V}_{in}$ the pressure and velocity in the fluid at the location of the particle due to the acoustic field, and $\langle\ \rangle$ denotes a time average. The factors f_1 and f_2 are given as

$$f_1 = 1 - \frac{c_f^2 \rho_f}{c_p^2 \rho_p}, \qquad f_2 = 2\left(\frac{\rho_p - \rho_f}{2\rho_p + \rho_f}\right).$$

The pressure and velocity can be written as a function of velocity potential ϕ (Barmatz and Collas, 1985)

$$P_{in} = -\rho_f \frac{\partial \phi}{\partial t} \tag{5}$$

$$\boldsymbol{V}_{in} = \nabla\phi. \tag{6}$$

We note that Chen and Apfel (1996) have recently derived force expressions in various axisymmeteric wave fields by integrating the Brillouin radiation tensor (the time-average momentum flux density tensor) over the particle surface. Doinikov (1994) has solved this hydrodynamic problem for an arbitrary-size sphere and included viscous effects.

The velocity potential due to planar stationary acoustic field around a solid cylinder can be represented as the sum of the incident and scattered field. Hasegawa et al. (1988) have developed a velocity potential for such a case. The velocity potential of the incident stationary plane wave in cylindrical coordinates is represented as the real part of

$$\phi_i = A\cos(\omega t) \sum_{n=0}^{\infty} \epsilon_n (-i)^n \delta_n J_n(kr)\cos(n\theta), \tag{7}$$

where

$$\epsilon_0 = 1 \qquad \text{and} \qquad \epsilon_n = 2 \ (n = 1, 2, 3, \ldots)$$

$$\delta_n = e^{-ikh} + (-1)^n e^{ikh}$$

and θ is the angle relative to the direction of propagation of the acoustic field (the y-coordinate in Figure 9). Also, A is the amplitude of the potential, h the distance between the nodal plane and the center of the cylinder, ω the radial frequency, and k the wavenumber. Note that $J_n(kr)$ is the cylindrical Bessel function of the first kind and order n, which represent standing waves in the cylindrical coordinate system. Using the simplified nomenclature

$$B_n = \epsilon_n (-i)^n \delta_n \qquad \text{and} \qquad \nu = kr,$$

the incident field potential can be written as

$$\phi_i = A\cos(\omega t) \sum_{n=0}^{\infty} B_n J_n(\nu)\cos(n\theta) \tag{8}$$

The scattered field potential is written as

$$\phi_s = A\cos(\omega t) \sum_{n=0}^{\infty} B_n d_n H_n^{(2)}(\nu)\cos(n\theta), \tag{9}$$

where $H_n^{(2)}$ is the Hankel function of the second kind and order n. The coefficients d_n are known functions of material properties of the cylinder and fluid, the radius of the cylinder, and the acoustic frequency (Hasegawa et al., 1988). Thus the total velocity potential around the cylinder is

$$\begin{aligned}\phi &= \phi_i + \phi_s \\ &= A\cos(\omega t) \sum_{n=0}^{\infty} B_n \cos(n\theta)[J_n(\nu) + d_n H_n^{(2)}(\nu)].\end{aligned} \tag{10}$$

Using Eqs. 5 and 6, the pressure and velocity expressions can be written as

$$P_{in} = A\rho_f \omega \sin(\omega t) \sum_{n=0}^{\infty} B_n \cos(n\theta)[J_n(\nu) + d_n H_n^{(2)}(\nu)]$$

$$\boldsymbol{V}_{in} = kA\cos(\omega t)$$

$$\times \left\{ \begin{array}{l} \left(\displaystyle\sum_{n=0}^{\infty} B_n \cos(n\theta)[J_n'(\nu) + d_n H_n^{(2)\prime}(\nu)] \right) \boldsymbol{e}_r \\ -\left(\displaystyle\sum_{n=0}^{\infty} nB_n \sin(n\theta)[J_n(\nu) + d_n H_n^{(2)}(\nu)]/\nu \right) \boldsymbol{e}_\theta \end{array} \right\},$$

where the prime indicates differentiation with respect to ν, and $\boldsymbol{e}_r$ and $\boldsymbol{e}_\theta$ are the unit vectors in cylindrical coordinates. Taking the time average of the square of pressure and velocity and inserting the result into Eq. 4, we can write the acoustic potential U as

$$U = 2\pi R_p^3 \rho_f A^2 k^2 \left\{ \frac{P_s}{6} f_1 - \frac{(V_{sr} + V_{s\theta})}{4} f_2 \right\}, \quad (11)$$

where

$$P_s = \left\{ \sum_{n=0}^{\infty} B_n \cos(n\theta) [J_n(\nu) + d_n H_n^{(2)}(\nu)] \right\}^2$$

$$V_{sr} = \left\{ \sum_{n=0}^{\infty} B_n \cos(n\theta) [J_n'(\nu) + d_n H_n^{(2)\prime}(\nu)] \right\}^2$$

$$V_{s\theta} = \left\{ \sum_{n=0}^{\infty} nB_n \sin(n\theta) [J_n(\nu) + d_n H_n^{(2)}(\nu)]/\nu \right\}^2.$$

We define a dimensionless potential U^* as

$$U^* = \frac{U}{4\pi R_p^3 E_{ac}} = \left\{ \frac{P_{sr}}{6} f_1 - \frac{(V_{sr} + V_{s\theta})}{4} f_2 \right\}, \quad (12)$$

which is used in Eq. 3 to calculate the primary acoustic force as follows:

$$F_{ac,x} = 4\pi R_p^3 E_{ac} k \left[\frac{\partial U^*}{\partial \nu} \sin\theta + \frac{1}{\nu} \frac{\partial U^*}{\partial \theta} \cos\theta \right] e_x \quad (13a)$$

$$F_{ac,y} = -4\pi R_p^3 E_{ac} k \left[\frac{\partial U^*}{\partial \nu} \cos\theta - \frac{1}{\nu} \frac{\partial U^*}{\partial \theta} \sin\theta \right] e_y. \quad (13b)$$

Hydrodynamic force

For the creeping flow about a circular cylinder (radius R_c) inserted transversely in a uniform flow, we use the approximate solution provided by Lamb (1932). The velocity components are given by

$$u_{f,x} = U_f \left\{ \frac{\ln(r/R_c) - 0.5(1 - R_c^2/r^2)\cos(2\vartheta)}{2.002 - \ln(Re_c)} \right\} \quad (14a)$$

$$u_{f,y} = -0.5 U_f \frac{(1 - R_c^2/r^2)\sin(2\vartheta)}{2.002 - \ln(Re_c)}, \quad (14b)$$

where

$$Re_c = \frac{2R_c U_f \rho_f}{\mu} \quad (15)$$

and ϑ is the angle measured with respect to the flow direction (the x-direction of Figure 9).

Trajectory equations

Combining Eqs. 13 and 14 with Eq. 2, the dynamic equations for the particle trajectories can be obtained. For ease of computation, we define dimensionless variables

$$x_p^* = x_p/R_c, \quad y_p^* = y_p/R_c, \quad r^* = r/R_c, \quad t^* = U_f t/R_c,$$

which lead to the dimensionless trajectory equations:

$$\frac{dx_p^*}{dt^*} = \frac{2Gk}{3} \left[\frac{\partial U^*}{\partial \nu} \sin\theta + \frac{1}{\nu} \frac{\partial U^*}{\partial \theta} \cos\theta \right] + \frac{\ln(r^*) - 0.5(1 - 1/r^{*2})\cos(2\vartheta)}{2.002 - \ln(Re_c)} \quad (16a)$$

$$\frac{dy_p^*}{dt^*} = -\frac{2Gk}{3} \left[\frac{\partial U^*}{\partial \nu} \cos\theta - \frac{1}{\nu} \frac{\partial U^*}{\partial \theta} \sin\theta \right] - 0.5 \frac{(1 - 1/r^{*2})\sin(2\vartheta)}{2.002 - \ln(Re_c)}. \quad (16b)$$

Here we have defined the Gor'kov number

$$Gk = \frac{R_p^2 k E_{ac}}{\mu U_f},$$

which is the ratio of acoustic to drag forces. Particle trajectories depend on the material characteristics of the fiber through the scattering coefficients d_n and the acoustic properties of the particles and fluid through the constants f_1 and f_2. Typical values of the dimensionless groups, for a 10-μm polystyrene particle in water ($\mu = 10^{-3}$ Pa·s, $\rho_f = 10^3$ kg/m^3) in the presence of an acoustic field with $E_{ac} = 4$ J/m^3 and $k \sim 4 \times 10^3$ and a flow speed of $U_f = 0.2$ cm/s around a 0.1-mm fiber are $Gk = 0.85$ and $Re_c = 0.4$. Thus, both acoustic forces and fluid inertia are significant under conditions typical of our experiments.

Values of material properties and geometrical dimensions used in the simulations are listed in Table 2. In order to illustrate the effect of collector material on the particle trajectories, we include simulations for the case of collectors made from aluminum as well as polyester fibers. In all cases, the simulation frequency was 1.0 MHz and the acoustic energy density ranged from 1.0 J/m^3 to 20.0 J/m^3.

The trajectory equations (Eqs. 16) were solved simultaneously using Mathematica on a personal computer. A simple Euler's method was used for integration with a step size of 0.25 dimensionless time units. The infinite series in Eq. 11 were terminated at the fifth term because the ratio d_0/d_4 is of the order of 10^{-7} and no noticeable differences were observed in the trajectories by keeping additional terms. Sets of particle trajectories were calculated using initial positions x_0

Table 2. Values of Material Properties and Geometrical Dimensions Used in the Trajectory Simulations

	Particle (Polystyrene)	Fiber (Polymer)	Fiber (Aluminum)	Fluid (Water)
Radius, m	10^{-5}	10^{-4}	10^{-4}	
Longitudinal sound speed, m/s	2,300	2,430	6,420	1,480
Shear sound speed, m/s		1,200	3,040	
Density, kg/m^3	1,050	1,230	2,700	1,000
Viscosity, Pa·s				10^{-3}

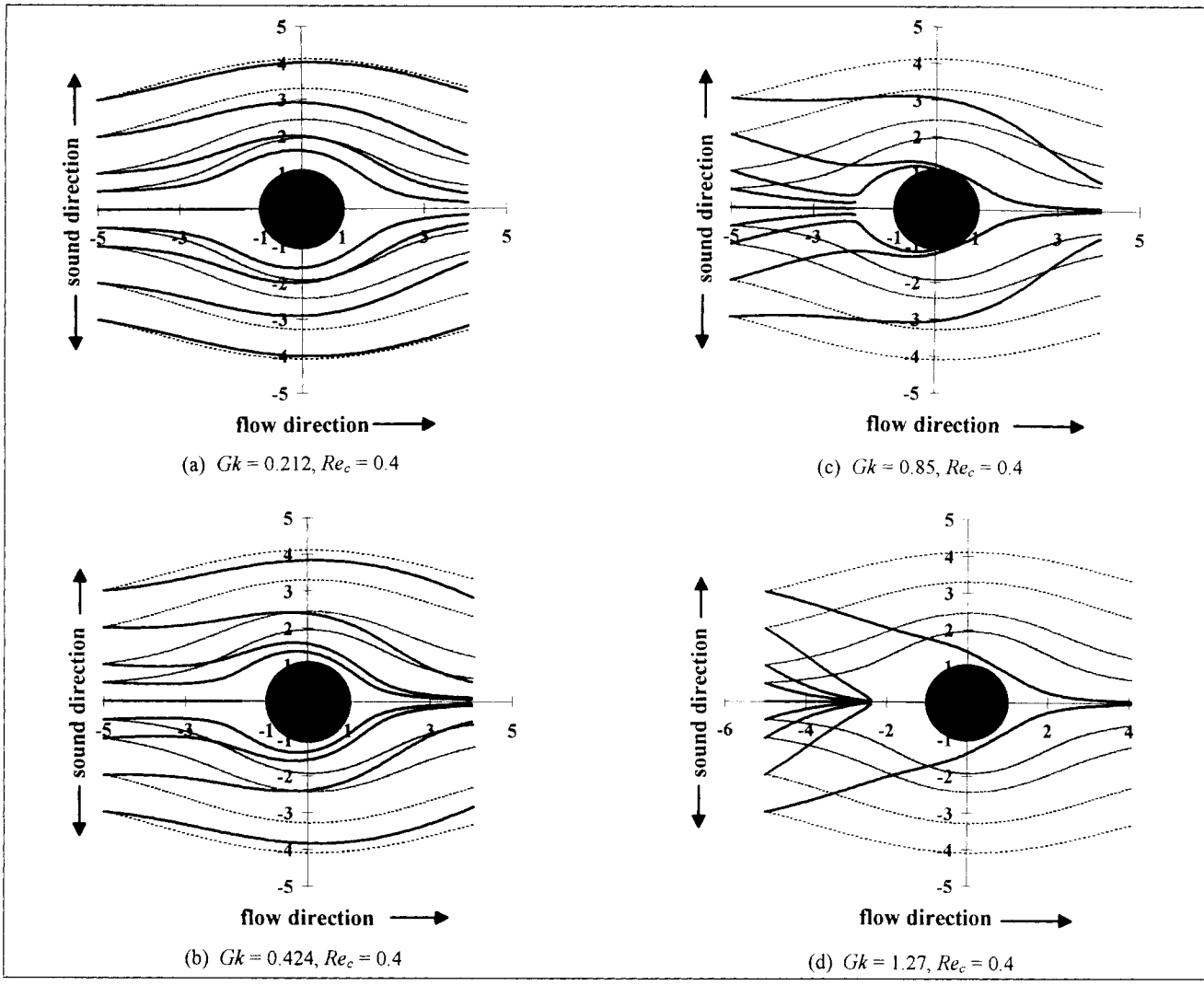

Figure 10. Simulated trajectories of polystyrene particles around a fiber located at the pressure node of the acoustic field at various *Gk* but fixed $Re_c = 0.4$.

Dashed lines indicate hydrodynamic pathlines, while solid lines indicate particle trajectories.

$= -5$ and $-3 \le y_0 \le 3$. The value $x_0 = -5$ was chosen because at this, and further distances from the fiber, fluid streamlines are unaffected by the presence of fiber. The simulation of the particle trajectory was continued until one of the following conditions was met:

1. The particle passed far beyond the fiber, $x_p^* \ge 4$.
2. The particle impinged onto the fiber, $r^* \le (1 + R_p/R_c)$. A more accurate definition of impingement would require the particle to have a nonzero radial velocity toward the collector (Weber and Paddock, 1983).
3. The particle velocity became small, that is, $|\tilde{u}_p^*| < 0.005$.
4. The number of integration steps exceeded 500.

One set of simulations was performed under the assumption that the center of the fiber coincided with the pressure node of the acoustic field. Figure 10 shows the particle trajectories for *Gk* in the range 0.212 to 1.27 and a fixed $Re_c = 0.4$. The dashed lines give particle trajectories due to hydrodynamic effects alone (no acoustic field), while the solid lines represent the predicted trajectories in the presence of the acoustic field. The trajectories are observed to bend toward the pressure node (horizontal plane through the center of the fiber) with the bending tendency increasing with an increase in *Gk*. This is expected since the primary acoustic force is expected to drive particles toward the node. At $Gk = 1.27$, there is a potential energy minimum around the point $(-2.5, 0)$, and many trajectories terminate there. This could explain the globular particle collection experimentally observed at some positions within the porous medium.

Figure 11 shows the particle trajectories under the conditions of higher Re_c. Comparison of the trajectories in Figure 11 with those in Figures 10b and 10c shows that the deviation from hydrodynamic trajectories is reduced with an increase in Re_c for a given *Gk*. Notice that the maximum acoustic force is expected to occur at $\lambda/8$ distance from the node (center of the collector), which corresponds to positions where $y = \pm 1.85$. As can be seen in the figure, the strongest deviation of particle trajectories from their hydrodynamic paths occurs in this vicinity.

In order to quantify the acoustically enhanced filtration phenomenon, filtration enhancement factors can be calculated by locating the critical particle trajectories that just miss

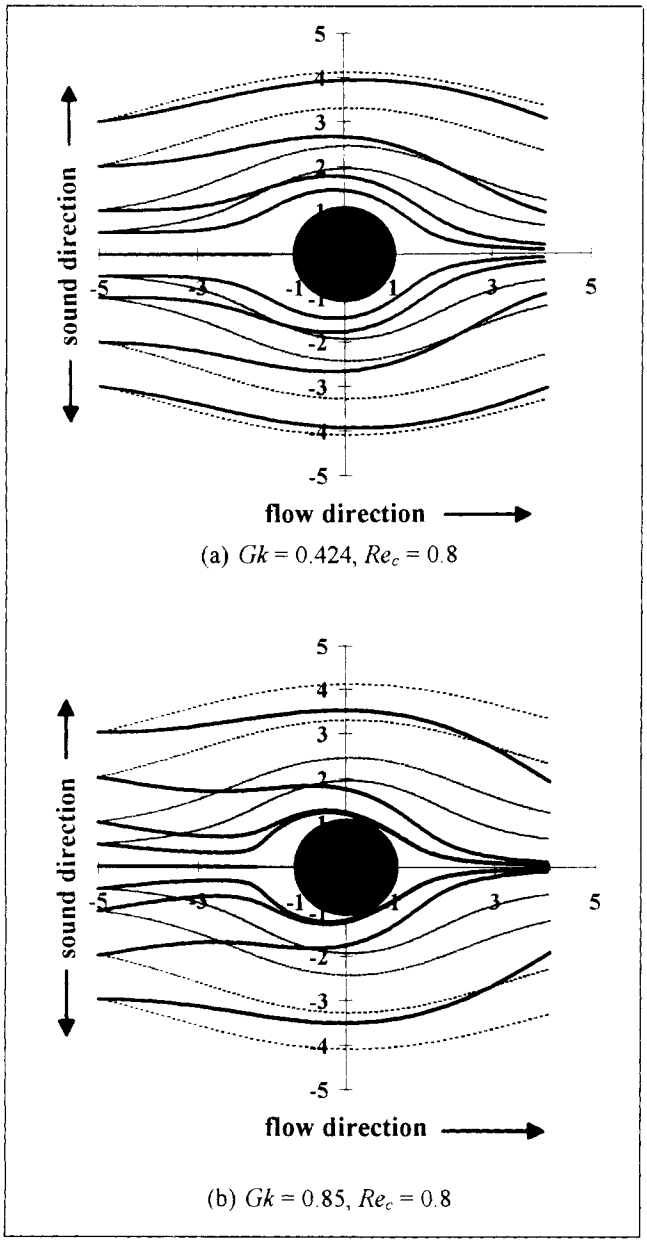

Figure 11. Simulated trajectories of polystyrene particles around a fiber located at a pressure node of the acoustic field for $Re_c = 0.8$.

the collector for given operating conditions. The initial coordinates y_0 for such critical trajectories were determined for a range of Gk and Re_c. To model the amount of collection due to hydrodynamic interception, similar critical trajectories were also identified for the case when $Gk = 0$. The latter was found to be very small (e.g., $y_0 \approx 0.008$). The ratio of these two values of y_0 represents a filtration enhancement factor attributable to the acoustic field. To represent the overall filtration efficiency, single-fiber collection efficiencies can be averaged over the whole porous medium, taking into account the fiber orientation and some probability arguments (Gerber and Birss, 1983). Figure 12 shows the position of the critical trajectory as a function of Gk for both aluminum and polyester collectors at two different values of Re_c. For a constant Re_c, the collection efficiency rises sharply with increasing Gk to a plateau value. As expected, the collection efficiency decreases with an increase in Re_c, but eventually reaches the same plateau when the acoustic field intensity is large enough (high Gk).

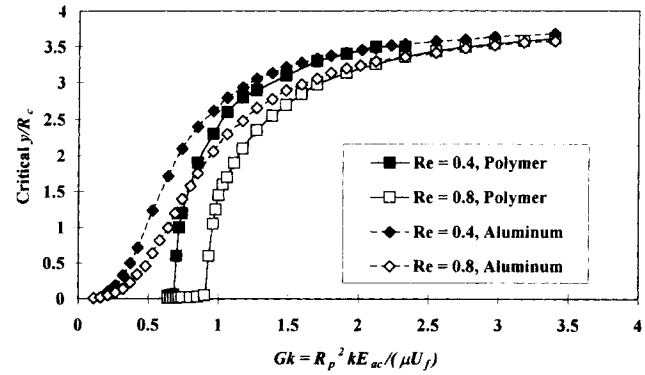

Figure 12. Initial position of critical collection trajectories as a function of Gk for two values of Re_c for aluminum and polymer collectors.

Figure 13 shows the simulation results for the case when the collector is $\lambda/8$ from a nodal plane. In this case, the particle trajectories tend to be focused together as the particles flow past this collector downstream toward the next. This focusing effect may explain the dendritic collection phenomenon observed in some experiments.

The simulations presented here cannot be directly related to the experimental results due to the complexity of the actual experiment (e.g., the porous medium is actually a connected web of fibers, and the experiment is inherently unsteady state since the particle concentration builds inside the porous medium). However, it does provide a qualitative picture of the filtration phenomenon. The trajectory analysis in-

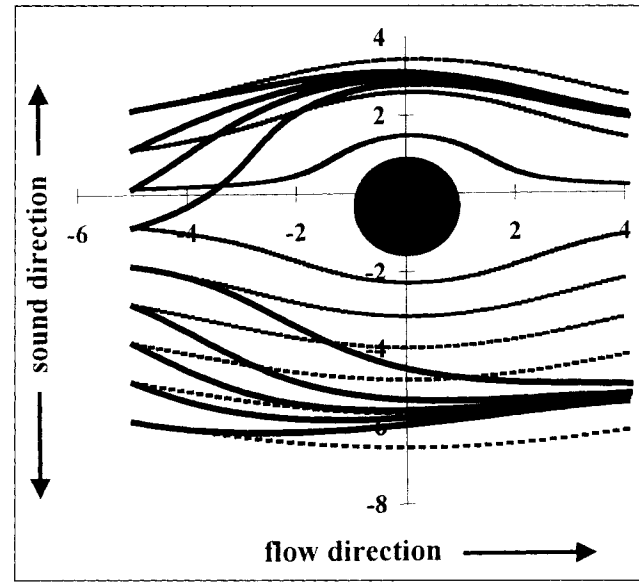

Figure 13. Simulated trajectories of polystyrene particles around fibers located at $\lambda/8$ from pressure node.

dicated that particles could be trapped in stationary positions around the fiber even though suspension flow is ongoing.

Summary and Conclusions

Resonant acoustic fields were successfully employed to enhance the filtration efficiency of a porous medium. Good collection efficiencies were achieved for the filtration of fine particulate suspensions through the polymeric foam having pores two orders of magnitude larger than the particles of suspension. The residence time required in the acoustically active chamber was short, ranging from 0.25 to 0.5 min for the experimental results reported here. Cumulative filtration efficiencies in excess of 60% were reached within 2 to 4 residence times of operation and could be maintained above 70% for 15 to 25 residence times. Eventually the porous medium becomes saturated with particles and instabilities in the collection phenomenon arise. It is possible that these instabilities are related to increased acoustic absorption by the collections of particles entrapped within the porous medium. Such localized heating can result in acoustic streaming, which would lead to a reduced efficiency for particle trapping. The time to saturation decreases almost proportionally to the particle loading in the feed, indicating that filtration is limited by the mass of solids retained inside the porous medium. Effects of different processing variables on filter performance were confirmed. The ease of operation, high filtration efficiency, and low-pressure drop associated with this new filtration approach allows it to be potentially useful for many practical applications.

The simplified particle-trajectory analysis captures the essential features of the filtration process. Acoustic forces can cause particle trajectories to deviate from hydrodynamic pathlines toward particle collectors, thereby enhancing their collection efficiency in comparison to pure hydrodynamic interception. The prediction of localized potential energy minima may explain the formation of particle clusters observed in the experiments. The predicted focusing of particle trajectories may be the origin of the dendritic particle collection observed in other cases.

Acknowledgments

The authors are grateful to both Nestle R&D and Kinetico Inc. for their partial support of this work.

Literature Cited

Allman, R., and W. T. Coakley, "Ultrasound Enhanced Phase Partitioning of Microorganisms," *Bioseparation*, **4**, 29 (1994).

Apfel, R. E., "Radiation Pressure—Principles and Application to Separation Science," *Fortschr. Acust. DAGA'90 Wien*, Wien, Austria, p. 19 (1990).

Barmatz, M., and P. Collas, "Acoustic Radiation Potential on a Sphere in Plane, Cylindrical, and Spherical Standing Wave Fields," *J. Acoust. Soc. Amer.*, **77**, 928 (1985).

Benes, E., F. Hager, W. Bolek, and M. Groschl, "Separation of Dipsersed Particles by Drifting Ultrasonic Resonance Fields," *Proc. Ultrasonics Int. Conf.*, published by Butterworth-Heinemann, Oxford, U.K., p. 167 (1991).

Biot, M. A., "Theory of Propagation of Elastic Waves in a Fluid-Saturated Porous Solid: I. Low-Frequency Range," *J. Acoust. Soc. Amer.*, **28**, 168 (1956a).

Biot, M. A., "Theory of Propagation of Elastic Waves in a Fluid-Saturated Porous Solid: II. High-Frequency Range," *J. Acoust. Soc. Amer.*, **28**, 179 (1956b).

Chen, X., and R. E. Apfel, "Radiation Force on a Spherical Object in an Axisymmetric Wave Field and Its Application to the Calibration of High-Frequency Transducers," *J. Acoust. Soc. Amer.*, **99**, 713 (1996).

Doblhoff-Dier, O., Th. Gaida, H. Katinger, W. Burger, M. Groschl, and E. Benes, "A Novel Ultrasonic Resonance Field Device for the Retention of Animal Cells," *Biotechnol. Prog.*, **10**, 428 (1994).

Doinikov, A. A., "Acoustic Radiation Pressure on a Compressible Sphere in a Viscous Fluid," *J. Fluid Mech.*, **267**, 1 (1994).

Frank, A., W. Bolek, M. Groschl, W. Burger, and E. Benes, "Separation of Suspended Particles by Use of the Inclined Resonator Concept," *Proc. Ultrasonics Int. Conf.*, published by Butterworth-Heinemann, Oxford, U.K., p. 519 (1993).

Gerber, R., and R. R. Birss, *High Gradient Magnetic Separation*, Research Studies Press, Chichester, NY (1983).

Gor'kov, L. P., "On the Forces Acting on a Small Particle in an Acoustic Field in an Ideal Fluid," *Sov. Phys. Dok.*, **6**, 773 (1962).

Gupta, S., D. L. Feke, and I. Manas-Zloczower, "Fractionation of Mixed Particulate Solids According to Compressibility Using Ultrasonic Standing Wave Fields," *Chem. Eng. Sci.*, **50**, 3275 (1995).

Gupta, S., and D. L. Feke, "Acoustically Driven Collection of Suspended Particles within Porous Media," *Ultrasonics*, **35**, 131 (1997).

Gupta, S., "Acoustically Driven Filtration of Particulate Suspensions in Porous Media," PhD Diss., Case Western Reserve Univ., Cleveland, OH (1997).

Hasegawa, T., K. Saka, N. Inoue, and K. Matsuzawa, "Acoustic Radiation Force Experienced by a Solid Cylinder in a Plane Progressive Sound Field," *J. Acoust. Soc. Amer.*, **83**, 1770 (1988).

Johnson, D. L., "Recent Developments in the Acoustic Properties of Porous Media," *Frontiers in Physical Acoustics*, North-Holland, Amsterdam, p. 255 (1986).

King, L. V., "On the Acoustic Radiation Pressure on Spheres," *Proc. R. Soc.*, **A147**, 212 (1934).

Lamb, H., *Hydrodynamics*, 6th ed., Cambridge Univ. Press, London (1932).

Mandralis, Z. I., and D. L. Feke, "Fractionation of Fine Particle Suspensions by Synchronized Ultrasonic and Flow Fields," *AIChE J.*, **39**, 197 (1993a).

Mandralis, Z. I., and D. L. Feke, "Continuous Suspension Fractionation Using Acoustics and Divided Flow Fields," *Chem. Eng. Sci.*, **48**, 3897 (1993b).

Mandralis, Z. I., W. Bolek, W. Burger, E. Benes, and D. L. Feke, "Enhanced Synchronized Ultrasonic and Flow-Field Fractionation of Suspensions," *Ultrasonics*, **32**, 113 (1994).

Peterson, S. C., U.S. Patent No. 4,759,775 (1988).

Schram, C. J., U.S. Patent No. 4,743,361 (1988).

Schram, C. J., and M. Rendell, "Manipulation of Particles in Megahertz Standing Waves," *Proc. Ultrasonics Int. Conf.*, p. 262 (1989).

Tolt, T. L., and D. L. Feke, "Separation Devices Based on Forced Coincidence Response of Fluid-Filled Pipes," *J. Acoust. Soc. Amer.*, **91**, 3152 (1992).

Tolt, T. L., and D. L. Feke, "Separation of Dispersed Phases from Liquids in Acoustically Driven Chambers," *Chem. Eng. Sci.*, **48**, 527 (1993).

Weber, M. E., and D. Paddock, "Interceptional and Gravitational Collision Efficiencies for Single Collectors at Intermediate Reynolds Numbers," *J. Colloid Interf. Sci.*, **94**, 328 (1983).

Whitworth, G., M. A. Grundy, and W. T. Coakley, "Transport and Harvesting of Suspended Particles Using Modulated Ultrasound," *Ultrasonics*, **29**, 439 (1991).

Yasuda, K., S. Umemura, and K. Takeda, "Concentration and Fractionation of Small Particles by Ultrasound," *Jpn. J. Appl. Phys.*, **34**, 2715 (1995).

Yosioka, R., and G. Kawasima, "Acoustic Radiation Pressure on a Compressible Sphere," *Acoustica*, **5**, 167 (1995).

Manuscript received Oct. 14, 1997, and revision received Mar. 2, 1998.